Experimental studies of flexocaloric effect in materials with structural phase transitions

Author: Clàudia Pérez-Junyent.
*Facultat de Física, Universitat de Barcelona, Diagonal 645, 08028 Barcelona, Spain.**

Advisor: Dr. Eduard Vives Santa-Eulalia

Abstract: The flexocaloric effect has been studied in a Cu-Al-Ni single crystal by inducing the martensitic phase transition with a three point bending setup. This transition has been monitored with infrared measurements, allowing to obtain maps of the sample surface temperature. These maps are processed by inverting the Fourier equation in order to obtain the evolution of heat sinks and sources associated with interphase front movement.

I. INTRODUCTION

The interest in refrigeration devices, alternative to standard cooling systems based on the liquid - gas phase transition has increased in recent years. The fluids needed for standard refrigeration, like chlorofluorocarbons, or hidrochlorofluorocarbons [1], that display a phase transition close to the room temperature, are known to contribute to the greenhouse effect in the atmosphere. Some of the alternatives that have been investigated are the solid-state cooling technologies and more precisely the use of the caloric effects shown by some materials [2].

The caloric effect is defined as the isothermal change of entropy or the adiabatic change of temperature when a generic external field is applied or released on a given material [1]. Examples are: magnetocaloric effects (magnetic field) [3], electrocaloric effects (electric field) [4] and mechanocaloric effects (mechanical stresses). Among the mechanocalorics case one distinguishes: barocaloric (pressure), elastocaloric (uniaxial stress) [2] and more recently flexocaloric (flexure or torsion) [5].
In general, to apply mechanical stresses it is easier than applying electric or magnetic fields. Although until recently lots of efforts have been put in barocaloric and elastocaloric effects, the new flexocaloric case is known to require smaller applied forces at the expense of larger displacements. This can be an advantage for some devices.

The materials that show a good mechanocaloric effect are those that exhibit a first order structural phase transition with large latent heats [6]. This occurs in the so called shape memory alloys like Cu-Al-Ni. These alloys display a structural phase transformation (also called martensitic). It is a first order solid-solid transition characterized by a symmetry change between a cubic phase (austenitic phase at high temperature or low stresses), and a monoclinic phase (martensitic phase at low temperature or high stresses). The transition, when cooling, proceeds by the nucleation and growth of monoclinic domains which occurs in an inhomogeneous and an intermittent manner also called avalanche dynamics [7] [8].

If the transition is induced by uniaxial stress, in isothermal conditions from the cubic to the monoclinic phase, the system evolves from a high symmetry phase with large atomic vibrations to a lower symmetry phase, more compact. In this phase transition the entropy decreases and the system releases latent heat to the environment. Inducing the transition in the opposite way (removing stress) implies an increment of the entropy so that the system absorbs heat from the environment.
If this process occurs very fast, in adiabatic conditions, the system cannot exchange heat with the environment and the application of stress results in a temperature increase of the sample, whereas the removal of the stress results in a temperature decrease. This is the caloric effect that wants to be exploited for the design of solid state cooling devices.

The aim of the present work is to characterize experimentally this temperature change by using infrared (IR) measurements of the surface temperature in a sample submitted to a three point bending experiment, which represents a more complex mechanism for inducing the structural phase transition than uniaxial stress. It is remarkable to notice that when bending a beam sample, the upper part of the sample is stretched and the lower part is compressed [5].

II. EXPERIMENT

The studied sampled is a single crystal with nominal composition $Cu_{67,7}Al_{26,7}Ni_{5,6}$ at.% [7], produced by Nimesis Technology (France). The sample dimensions are 110 mm × 5 mm × 1 mm. According to the manufacturer the long symmetry axis is oriented along <100> crystallographic direction of the cubic phase. The sample transforms from the cubic phase to a 18R martensitic phase (monoclinic). When cooling, at zero stress the transition starts $M_S = 258 \pm 1\,\mathrm{K}$. When applying uniaxial stress at room temperature, the transition starts at $\sigma_T = 90 \pm 5\,\mathrm{MPa}$ [7].

*Electronic address: clperezj7@alumnes.ub.edu

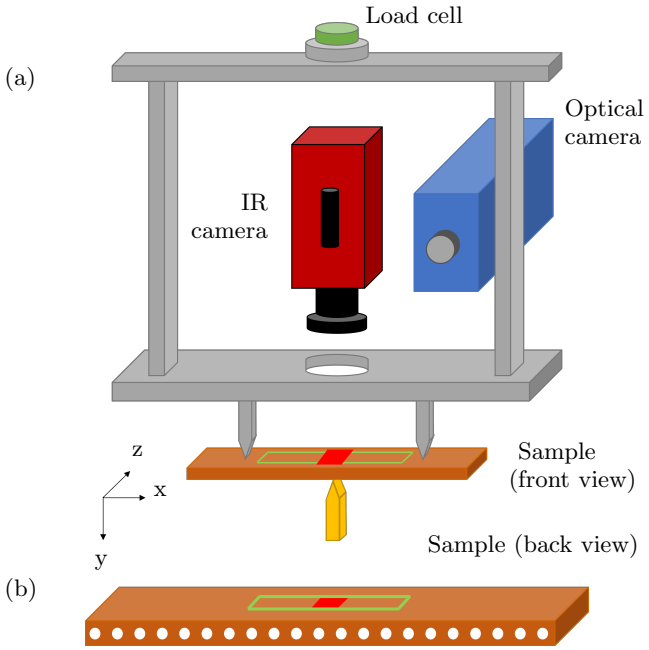

FIG. 1: (a) Diagram of the experimental setup showing the position of the sample, the pins of the three point bending test, the IR camera, the optical camera and the load cell. (b) Detail of the sample showing the 21 white dots (separated 0.5 cm) used for the discretization of the sample profile.

A schematic representation of the experimental setup is shown in FIG. 1 (a). The sample is bended and unbended in a three point inverted bending flexural test using a Zwick/Roell Z005 testing machine. This materials testing machine is equipped with a 5 kN load cell with a resolution of 0.5 N. The displacement of the upper pins with a resolution of 0.1 mm is controlled at an imposed constant speed.
The horizontal separation between the upper pins and the central lower pin is 30 mm. The two upper pins are made of metal while the lower one is made of plastic to reduce the thermal losses in the middle of the sample during the experiment. The materials testing machine is also equipped with an optical high precision camera with a CCD chip (768 × 756 pixel). It allows us to track the experiment at 5 images/s.

An infrared camera (InfraTec 8800) is positioned above the sample, as shown in FIG. 1 (a). A convenient hole in the three point bending frame allows to obtain IR images of the upper part of the sample, that has been covered with black matte paint to reduce the radiation reflection from the environment. Moreover the whole experiment has been surrounded by a thermal insulator polystyrene shield, ensuring a homogeneous temperature in the sample environment. The IR camera has a spatial resolution of Δx =18.3 pixel/mm, a temporal resolution of Δt =0.01 s/frame and the temperature resolution is 35 mK. The materials testing machine also measures the vertical position of the upper pins and the applied force that can be recorded simultaneously with the temperature maps.

III. RESULTS

A. Mechanical response

A first test at 500 mm/min has been performed in order to characterize the mechanical behaviour of the sample. In a first section of the test (bending) the upper pins descend down to a maximum amplitude of 25 mm. In the second section (unbending) the upper pins return to the initial position at 0 mm. The 16 frames captured with the optical camera during the bending section have been manually digitalised to get the point coordinates of a collection of white dots painted on the sample edge as represented in FIG. 1 (b). Since this digitalisation was done manually, the errors of the horizontal and vertical position is 1 mm. FIG. 2 shows the obtained profiles of the sample.

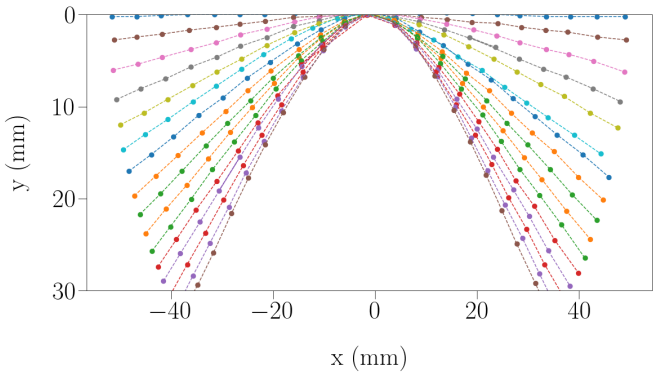

FIG. 2: Sample profile during the bending section with an amplitude of 25 mm and a velocity of 500 mm/min. The profiles are separated 0.2 s. It is noteworthy that the vertical axis is reversed compared to standard x-y plots.

FIG. 3 shows the behaviour of the force vs the vertical position during bending-unbending experiment at a very slow speed of 1 mm/min and down to a maximum amplitude of 35 mm. Doing the experiment at a very slow speed allows to improve the resolution of the force measurement.

After an initial elastic part, the system displays a yield point in which the force reaches a maximum value of 8.18±0.1 N, followed by an approximated linear decrease of the force. This effect is due to the occurrence of the structural phase transition. When the velocity is reversed, in order to start the unbending section there is a hysteresis of ∼1.8±0.1 N. It has been checked that this hysteresis is not related to the friction between the pins and the sample by comparing the experiment with oil and different sample roughness. Therefore, it is due to forces acting on the phase fronts, we speculate this could be due to quenched disorder in the sample (impurities, vacancies or dislocations).
In the last part of unbending section, the elastic linear segment is recovered again and the transition is completely reversed without any kind of plastic deformation.

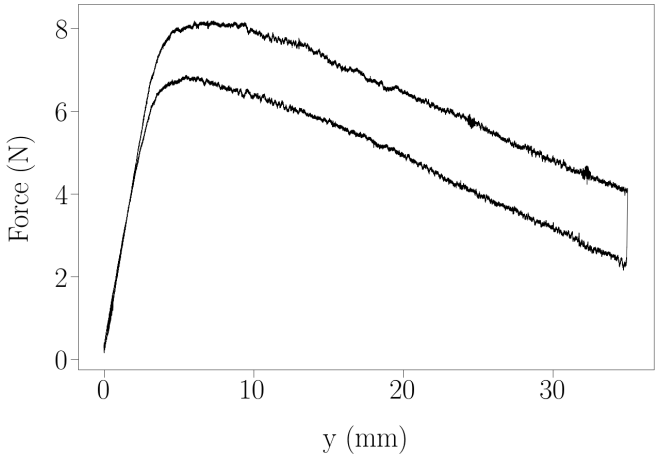

FIG. 3: Hysteresis cycle (force vs amplitude) obtained at a slow speed of 1 mm/min.

B. Thermal response

For the characterization of the thermal response of the sample a similar bending - unbending test has been performed at a high speed of 2000 mm/min and down to a maximum amplitude of 35 mm. This fast experiment corresponds to approximately adiabatic conditions and maximizes the temperature change of the sample. A pause of 120 s separates the two sections in order to allow a thermal equilibrium of the sample with the environment. In this case, the force resolution is worse due to the high speed of the experiment.

The temperature measurement with the IR camera is performed in the middle part of the sample as shown in FIG. 1 (a). For further analysis only a thin central section of the sample is studied in order to avoid edge and missfocusing effects. This section is represented with green lines in FIG. 1 (a) and (b). Moreover, we have also measured the central temperature of the sample by averaging the temperatures of a small area of 20 × 20 pixels as represented in FIG. 1 (a) and (b) with a red square.

FIG. 4 shows the evolution of the central temperature and the force response during the bending section ((a) and (b)) and unbending section ((c) and (d)). The panels (a) and (c) represent the amplitude evolution of the upper pins in the testing machine. The vertical dashed lines correspond to the beginning and ending of the pin movement. In panels (b) and (d) it is represented the evolution of the force in green (left vertical scale) and the evolution of the central temperature of the sample in red (right vertical scale).

For the bending section the central temperature starts to increase when the force is applied, approximately one second after the start of the pin movement the sample reaches its maximum value of overheating at 298.5 K and after that it tends to thermalise to room temperature.
A similar effect is seen in the unbending section, the central temperature decreases when the mechanic field is released and the sample reaches its minimum value at 292.0 K.

Comparing the force needed for the bending and unbending sections, one can see that the bending force is higher than the unbending one, this is due to the hysteresis cycle previously explained and shown in FIG. 3. It is also remarkable that the force needed for a $\Delta T \approx 3.0$ K thermal change in the central part of the sample is less than 10 N.

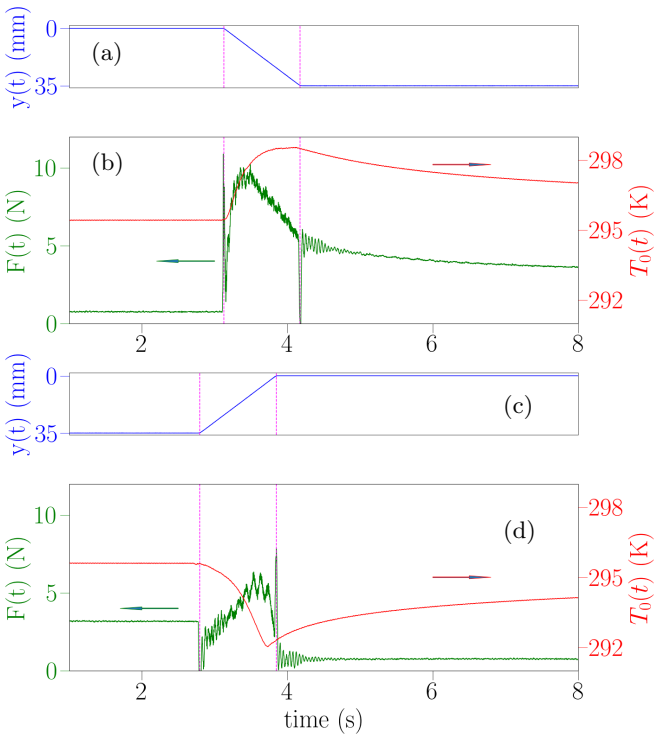

FIG. 4: Curves of the amplitude (in blue), the force (in green) and the temperature (in red) of the bending section ((a) and (b)) and unbending section((c) and (d)) with an amplitude of 35 mm and a 2000 mm/min velocity.

C. Thermal profiles

In the previous section the sample temperature has been measured as an average in the central part. In this section we concentrate on the study of the inhomogeneous temperature profile along the sample.
Despite the efforts in avoiding external IR radiation and thermal fluctuations of the environment, the temperature measurement still shows noise that can be avoided by a numerical smoothing treatment.
First, few pixels display a recorded temperature out of reasonable range due to electronic errors in the measurement. They are corrected with the average of the four neighbouring pixels. Moreover a 1D temperature profile along 640 pixels in the x-direction, is obtained by averaging the two dimensional data in the green rectangle shown in FIG. 1 (a) and (b) along the 128 pixels of the z-direction.

The temperature inhomogeneities in the sample will be a consequence of the moving phase transition fronts that absorb or release heat. We expect that the position of the these fronts is well defined and corresponds to rather sharp heat sinks and sources moving along the sample. The numerical analysis that will be performed in next section D. requires to smooth the data by performing an extra averaging. This cannot be done with a uniform running average because it will widen the phase fronts. Instead it should be performed with a Gaussian filter that respects the sharpness of the temperature inhomogeneities [9]. The details of this average are discussed in the Appendix. It allows to obtain smoothed temperature profiles $\bar{T}(i,k)$ where i represents the spatial pixels and k represents the temporal frames.

The evolution of the smoothed temperature profile is shown in FIG. 5 ((a) and (b) for the bending and unbending sections respectively. Colours indicate the surface temperature as shown in the scale at the bottom. Contour levels are plotted every 0.3 K, the vertical dashed lines indicate the beginning and end of the pin movement. Note that the maximum overheating and undercooling occurs close to the sample center, slightly before the pins stop moving. This caloric effect is a consequence of the martensitic phase transition. During the bending section, the overheating is caused by the moving martensitic phase fronts (from the center to the edges) which emit latent heat. Whereas during the unbending section the undercooling is due to the reversed movement of the cubic phase fronts which absorb latent heat. The maximum overheating and the minimum undercooling are a consequence of two competing effects: the velocity of the transition and the thermal conduction.

The final evolution after the pin movement stops correspond to a pure thermal relaxation due to heat conductivity of the sample towards the upper pins (metallic) and the central lower pin (which is made of plastic and less thermal conducting).

D. Heat sink & source location

A numerical processing of the temperature data should allow us to locate the positions of the fronts of the transformation that absorb or emit heat [7] [9].
Neglecting heat losses towards the air, heat transport can be described by the 1D Fourier equation:

$$\Sigma(x,t) = \frac{\sigma(x,t)}{C\rho} = \frac{\partial T(x,t)}{\partial t} - \frac{\kappa}{C\rho}\frac{\partial^2 T(z,t)}{\partial z^2} \qquad (1)$$

where Σ is the power source density (positive values) or the power sink density (negative values), σ is the heat production term, C is the sample specific heat, ρ is the density and κ is the thermal conductivity.

The Fourier equation (1) can be written in a discrete version for a better understanding of the numerical process. Replacing the spatial coordinate by $x = i\Delta x$ and the temporal coordinate by $t = k\Delta t$:

$$\Sigma(i,k) = \frac{1}{\Delta t}\frac{\partial \bar{T}(i,k)}{\partial k} - \frac{\kappa}{C\rho\Delta z^2}\frac{\partial^2 \bar{T}(i,k)}{\partial i^2} \qquad (2)$$

Note that the smoothed profiles are used for this numerical analysis. For the computation of the first temporal derivative and the second spatial derivative, the five point stencil method was used with increments of 20 frames and 30 pixels respectively:

$$\frac{\partial \bar{T}(i,k)}{\partial k} \approx \frac{1}{12\cdot 20}\big[-\bar{T}(i,k+40) + 8\bar{T}(i,k+20) - \\ - 8\bar{T}(i,k-20) + \bar{T}(i,k-40)\big] \qquad (3)$$

$$\frac{\partial^2 \bar{T}(i,k)}{\partial i^2} \approx \frac{1}{12\cdot 30^2}\big[-\bar{T}(i+60,k) + 16\bar{T}(i+30,k) - \\ -30\bar{T}(i,k) + \bar{T}(i-30,k) - \bar{T}(i-60,k)\big] \qquad (4)$$

Using the physical parameters for the Cu-Al-Ni alloy obtained from the literature [7], $\rho = 7120\,\mathrm{kg\,m^{-3}}$, $C = 450\,\mathrm{JK^{-1}kg^{-1}}$ and $\kappa = 45\,\mathrm{Wm^{-1}K^{-1}}$ the spatial and temporal dependence of Σ has been computed. Results are shown in FIG. 5 (c) and (d) for bending and unbending respectively. Note that only the temporal window of the pin motion is displayed (indicated by the vertical dashed lines).

Colors indicate the value of the power source density as shown in the color bar at the bottom. The units of Σ are K/s since the heat production term (σ) in $\mathrm{Wm^{-3}}$ is divided by the coefficient $C\rho$ in $\mathrm{JK^{-1}m^{-3}}$. Contour lines are separated 0.3 K/s.

Notice that when there is no pin movement (outside the dashed lines) Σ is almost zero. During the bending section (FIG. 5 c) a first heat source appears in the center of the sample reaching a value grater than 14 K/s and splits in two fronts that move towards the edges of the sample. During the unbending section (FIG. 5 d) the two fronts move from the edges towards the center, producing the undercooling with a value less than -12 K/s. It is relevant to be aware of the existence of a heat source at the end of the unbending section, which is due to the bottom pin, that favours the heat absorption of heat in the central location.

IV. CONCLUSIONS

We have studied the flexocaloric effect in a Cu-Al-Ni sample, which has been analysed in a three point bending inverted experiment. The profile of the sample has been characterized as well as its mechanical and thermal behaviour. As expected, a hysteresis cycle is obtained in the force-amplitude representation. It is found that the flexocaloric effect needs smaller forces than other mechanocaloric effects. A force applied of 10 N induces a thermal change of $\sim$3.0 K in the sample.

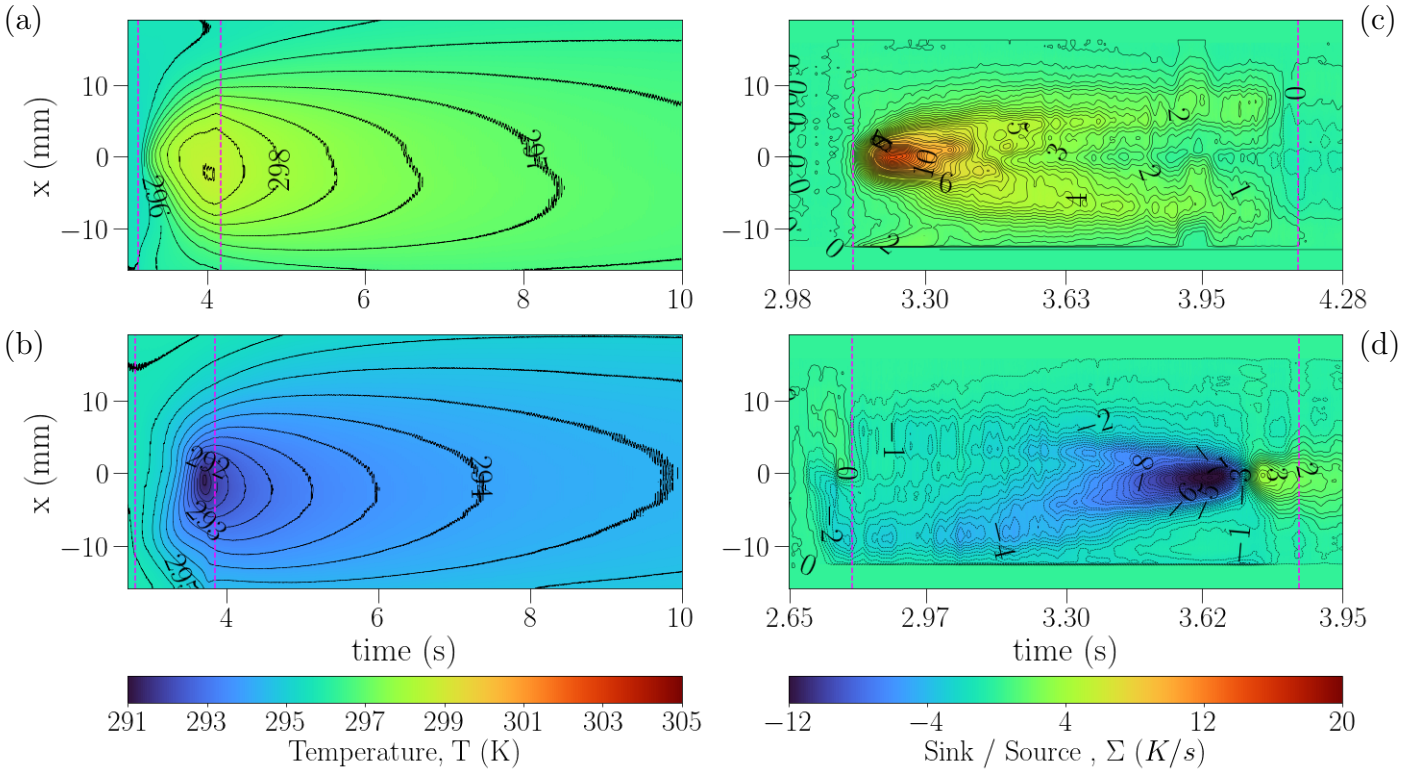

FIG. 5: (a) Temperature profile evolution as a function of time at a bending section of 2000 mm/min. (b) Equivalent data corresponding to the unbending section. (c) Heat source evolution for the bending section. (d) Heat sink evolution for the unbending section. Note that in (c) and (d) the temporal scale is magnified to show only the pin movement.

Evolution of the surface temperature profiles have been obtained by IR imaging, after a proper filtering of the experimental noise. A Fourier-based analysis allows to obtain the position of the heat sources and sinks.
The maximum thermal change is found at the center of the sample, where the largest bending occurs. This also coincides with the maximum value of the power source/sink density Σ for the bending and unbending sections.
The central temperature change for the bending section is $\Delta T \sim 3.0\,\mathrm{K}$; while the value for the unbending section $\Delta T \sim$-3.6 K.
In general, we have shown that the flexocaloric effect in solid materials is a good candidate for environmentally friendly and energetic efficient way of refrigeration.
As a natural extension of the present work, it would be noteworthy to study the behaviour of the flexocaloric effect for different bending velocities and different amplitudes.

Acknowledgments

This project was supervised by E.Vives. The author also wants to thank the patience and support received from close family and friends.

[1] L.Mañosa and A.Planes, *Materials with Giant Mechanocaloric Effects: Cooling by Strength*, Adv. Mater. **29**, 1603607 (2017).
[2] J.Tusek, K.Engelbercht, R.Millán-Solsona, L.Mañosa, E.Vives, L.P.Mikkelsen and N.Pryds, *The Elastocaloric Effect: A Way to Cool Efficiently*, Adv. Energy Mater. **5**, 1500361 (2015).
[3] A.M.Tishin and Y.I.Spichkin, *The Magnetocaloric Effect and its Applications*, Institute of Physics Publishing, Bristol, UK (2003).
[4] F.Le Goupil, J.Bennett, A.-K.Axelsson, M.Valant, A.Berenov, A.J.Bell, T.P.Comyn and N.McN. Alford, *Electrocaloric enhancement near the morphotropic phase boundary in lead-free NBT-KBT ceramics*, Appl. Phys. Lett. **107**, 172903 (2015).
[5] M.Porta, T.Castán, A.Saxena and A.Planes, *Flexocaloric effect near ferroelastic transition*, Phys. Rev. B **104**, 094108 (2021).
[6] E.Bonnot, R.Romero, L.Mañosa, E.Vives and A.Planes, *Elastocaloric Effect Associated with the Martensitic Transition in Shape-Memory Alloys*, Phys. Rev. Lett. **100** 125901 (2008).
[7] L.Iannicello, M.Romanini, L.Mañosa, A.Planes, K.Engelbercht and E.Vives, *Tracking the dynamics of power sources and sinks during the martensitic transformation of Cu-Al-Ni single crystal*, App. Phys. Lett. 10.1063/50006859 (2020).
[8] E.Vives, J.Ortín, L.Mañosa, I.Ràfols, R.Pérez-Magrané and A.Planes, *Distribution in avalanches in martensitic transformations* Phys. Rev. Lett. **72**, 1694 (1994).
[9] G.Capellera, L.Iannicello, M.Romanini and E.Vives, *Heat sink avalanche dynamics in elastocaloric Cu-Al-Ni single crystal detected by infrared calorimetry and gaussian filtering*, App. Phys. Lett. 10.1063/5.0066525 (2021).

V. APPENDIX

In this section we discuss the criteria followed for choosing the appropriate Gaussian filtering in order to locate the front position. The Gaussian filter of the temperature profile T(i,k) is defined as

$$\bar{T}(i,k) = \sum_{n=-4M}^{4M} T(i,k+n)G_n(M) \tag{5}$$

where $\bar{T}(i,k)$ is the filtered temperature profile, M is the width of the Gaussian kernel and G_n is the Gaussian distribution defined as:

$$G_n(M) = \frac{1}{\sqrt{2\pi M^2}} e^{-\frac{n^2}{2M^2}} \tag{6}$$

where M is a parameter controlling the width (in pixels) of the Gaussian kernel. The contribution of the Gaussian filtering is truncated for pixels farther than ±4M. In this work we have followed a different smoothing strategy compared to that in [9].

A study of the parameter M is necessary. If M is too small, the data will have too many fluctuations and will not allow for the correct computations of the derivatives in (3) and (4). If M is too large the details of the moving fronts will vanish.

FIG. 6 shows an example of the computed heat sink profile corresponding to t = 3.35 s for different values of M$\in (0, 10)$. Only a small interesting zone is represented, that corresponds to one front of the martensitic phase. Note that the value of Σ is negative because these profiles correspond to the heat sink (FIG. 5 d).

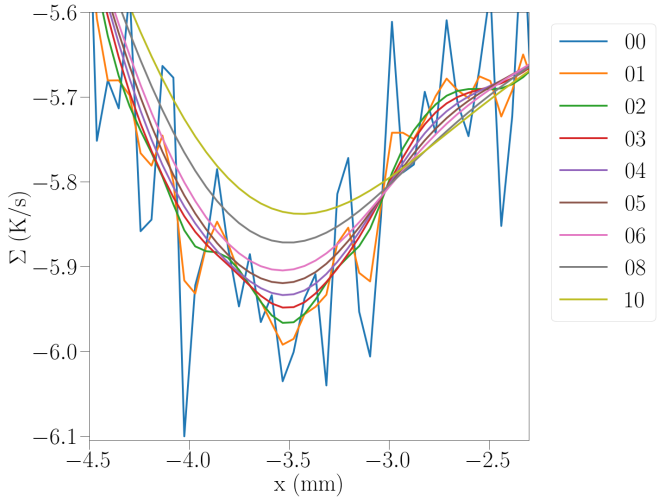

FIG. 6: Profile of the heat sink at t=3.35 s (unbending section of the experiment at 2000 mm/min and 35 mm of amplitude) for different values of M in the Gaussian filtering, those are represented in the legend.

The criteria followed to choose the best value of M is to reduce fluctuations as much as possible without increasing the value of the heat sink depth.

A value of M=4 is the chosen one for being applied to all the analysis of the experiments explained in the main work.